Simultaneous Segmentation and Motion Estimation in 4D–CT Data Using a Variational Approach

Jan Ehrhardt, Alexander Schmidt–Richberg and Heinz Handels

Department of Medical Informatics, University Medical Center Hamburg–Eppendorf, Hamburg, Germany

ABSTRACT

Spatiotemporal image data sets, like 4D CT or dynamic MRI, open up the possibility to estimate respiratory induced tumor and organ motion and to generate four-dimensional models that describe the temporal change in position and shape of structures of interest. However, two main problems arise: the structures of interest have to be segmented in the 4D data set and and the organ motion has to be estimated in the temporal image sequence.

This paper presents a variational approach for simultaneous segmentation and registration applied to temporal image sequences. The proposed method assumes a known segmentation in one frame and then recovers non-linear registration and segmentation in other frames by minimizing a cost function that combines intensity-based registration, level-set segmentation as well as prior shape and intensity knowledge. The purpose of the presented method is to estimate respiration induced organ motion in spatiotemporal CT image sequences and to segment a structure of interest simultaneously.

A validation of the combined registration and segmentation approach is presented using low dose 4D CT data sets of the liver. The results demonstrate that the simultaneous solution of both problems improves the segmentation performance over a sequential application of the registration and segmentation steps.

Keywords: segmentation, registration, 4D CT, respiratory motion, liver

1. PURPOSE

The main objective of radiation therapy is to eradicate or shrink tumor cells without damaging the surrounding tissue by delivering a high radiation dose to the tumor region and a dose as low as possible to neighboring normal tissues. Intrafraction organ motion is an issue that is becoming increasingly important for radiotherapy treatments. Especially, respiratory motion is characterized by a large magnitude and presents significant challenges in ensuring precise delivery of high radiation to thoracic and abdominal tumors. In conventional radiation therapy, safety margins are enlarged to compensate for respiratory motion. One the one hand, this solution increases the volume of irradiated healthy tissue so that the likelihood of treatment-related complications becomes larger. On the other hand, it limits attempts to escalate the dose delivered to the tumor to increase tumor control. In order to improve dose conformity and achieve steep dose gradients, recently a variety of techniques to explicitly account for respiratory motion has been proposed (breath-hold and shallow-breathing methods, respiratory gated techniques or respiration-synchronized techniques).[1] However, implementation and optimization of such techniques require detailed knowledge about respiratory motion and its impact on the dose delivery and resulting dose distributions.

Standard three-dimensional (3D) imaging does not provide information about the dynamic behavior of inner organs. In contrast, spatiotemporal image data sets, like 4D CT or dynamic MRI, open up the possibility to estimate respiratory induced tumor and organ motion and to generate four-dimensional models that describe the temporal change in position and shape of structures of interest. In radiotherapy of the thorax and upper abdomen, such models can be used to optimize radiotherapy plans in order to be less sensitive to breathing-induced organ motion and to enable respiratory gating or robotic radiotherapy.[1–3] However, two main problems arise: the structures of interest have to be segmented in the 4D data set and the organ motion has to be estimated by registering the frames in the temporal image sequence.

In our project, 4D CT image data with high spatial and temporal resolution is used to analyze the influence of the breathing motion on radiation dose distributions. For the calculation of organ specific dose distributions,

a segmentation of the structures of interest is necessary as well as an estimation of dense displacement fields to sum up the applied dose per voxel. The segmentation of inner organs in 4D CT data is a challenging problem, because in contrast to diagnostic CT protocols the exposure per slice has to be significantly reduced due to the large number of slices. Therefore, the resulting 4D images are characterized by a poor soft tissue contrast. We address this problem by using shape prior information for segmentation. Furthermore, from earlier work it is known that respiratory motion causes complex deformations of inner organs,[4] therefore a non-linear registration approach is required to estimate the deformation field.

Different approaches exist for modeling organ motion by solving the segmentation and registration problem independently,[5] by using the segmentation results to guide the registration process,[6–8] or by using the registration results to transfer an initial segmentation to all time frames.[4,9] However, solutions of both problems depend on each other. Therefore, some more recent methods embark on the strategy of solving the problems of motion estimation and segmentation simultaneously.

Many of these approaches, however, are not suitable for the segmentation and motion analysis of 4D medical images. Some of these approaches are restricted to lower dimensional parametric transformations[10–15] or are requiring specific atlas information.[16,17] A broad variety of methods use variational approaches based on level set segmentation and non–linear registration.[18–21] Some approaches are using level set based motion competition techniques.[18] However, the assumption of piecewise homogeneous motion does not hold for soft tissue deformations. In other approaches the estimated motion field is computed only at object surfaces[19,20] or no shape–prior information can be incorporated in the model.[20–22]

In this paper, we present a framework for combined intensity–based non–linear registration and level set based image segmentation that incorporates prior shape knowledge and prior intensity information. The segmentation is obtained by a non–linear registration to a reference shape and using a level set formulation related to the Mumford–Shah functional.[23] A global, dense displacement field is calculated using intensity and segmentation information. Both problems are formulated in a joint variational approach and solved simultaneously. We use the proposed method for the segmentation and respiration induced motion estimation of the liver in spatiotemporal CT image sequences. The reason for the choice of this particular application is two–fold: In context of an ongoing project[5,24,25] we want to compare simulated dose distributions for the conventional and respiratory gated irradiation of liver tumors. Moreover, the segmentation of the liver in CT images is challenging due to the poor soft tissue contrast and overlapping gray-level ranges of nearby tissues. For these reasons, conventional segmentation methods cannot be directly applied to liver segmentation. A variety of interactive and automatic liver segmentation approaches were developed in the last years,[26–29] though only few are applicable for low dose 4D CT images.[30]

The organization in this paper is as follows. In section 2.1 we present a variational approach for level set based segmentation using intensity and shape prior knowledge. Then, our way to combine segmentation and non–linear registration is explained in section 2.2. The numerical method to minimize the resulting energy functional is outlined in section 2.3. An experimental validation of the combined registration and segmentation approach is presented in section 3. First, we describe the 4D image data and the evaluation methods (section 3.1). The quantitative results in section 3.2 demonstrate that the simultaneous solution of both problems within a single mathematical framework improves the segmentation performance over a sequential application of the registration and segmentation steps.

2. METHODS AND MATERIALS

The purpose of the method proposed in this paper is to estimate a dense displacement field and simultaneously to segment a structure of interest (here: liver) in spatiotemporal CT image sequences. Our variational approach makes use of level set based segmentation models[31–33] and variational image registration techniques.[34] Due to poor soft tissue contrast in 4D CT data sets, prior shape and intensity knowledge will be included in the model.

Given is a spatio–temporal image sequence $I(\boldsymbol{x}, t) : \Omega \times I\!\!R \to I\!\!R$. We presume a reference shape for the segmentation of the object of interest in one of the image frames, let's say $I(\boldsymbol{x}, t_{ref})$. This reference segmentation is represented by a level set function $\Phi_{ref}(\boldsymbol{x}) : \Omega \to I\!\!R$ and is determined by a previous semiautomatic segmentation step. We seek for a each given time t_j the displacement vector field $\boldsymbol{u}_j(\boldsymbol{x}) : \Omega \to \Omega$ that describes
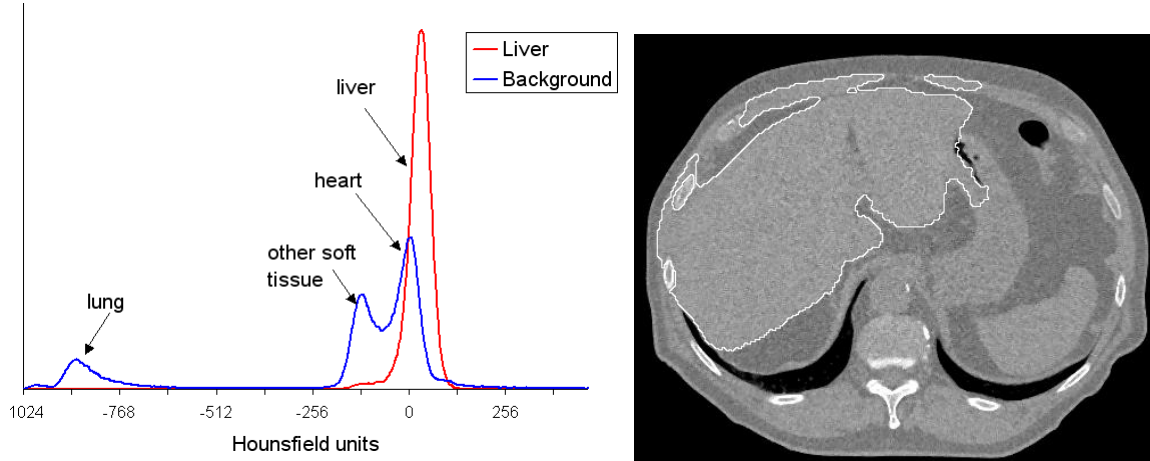
Figure 1. Left: Estimated gray value density functions for background and liver. Right: result of a intensity–based level set segmentation of the liver without shape prior information

the shift of position $\boldsymbol{x}$ in frame $I(\boldsymbol{x}, t_j)$ to its corresponding location in the reference frame $I(\boldsymbol{x} - \boldsymbol{u}_j(\boldsymbol{x}), t_{ref})$. Simultaneously, we seek the set of level set functions $\Phi_j(\boldsymbol{x})$ that represent the segmentation of the object of interest in the image frames.

2.1 Variational level–set segmentation using intensity and shape priors.

Since their introduction in the early 90's level set methods have become increasingly popular for image segmentation and have been utilized in many medical applications, e.g. for the segmentation of the liver[30] or the heart.[12] An important class of these methods uses region–based segmentation schemes by partitioning the image in homogeneous regions by fitting statistical intensity or texture models.[33, 35, 36] In contrast to edge–based models,[31, 32] region–based techniques tend to be less sensitive to noise and generate satisfactory results even if edge information is not present along the entire object boundary. Region-based segmentation algorithms commonly use an energy term based on Mumford-Shah segmentation functional[23] so that piecewise-constant intensity values are assumed. Available a priori knowledge about intensity properties of object and background can be incorporated by using precalculated density functions $p_{obj}(I)$ and $p_{bg}(I)$.[12] In our application, the region–based energy term is defined as:

$$\mathcal{J}^{Seg}[\Phi_j] = \int_\Omega \underbrace{-H(\Phi_j(\boldsymbol{x})) \log\left(p_{bg}(I(\boldsymbol{x}, t_j))\right)}_{\text{background region}} - \underbrace{(1 - H(\Phi_j(\boldsymbol{x}))) \log\left(p_{obj}(I(\boldsymbol{x}, t_j))\right)}_{\text{object region}} \ d\boldsymbol{x} + \int_\Omega \underbrace{\|\nabla H(\Phi_j(\boldsymbol{x}))\|}_{\text{contour length}} \ d\boldsymbol{x}$$

(1)

where $\Phi_j : \Omega \to \mathbb{R}$ is the desired level set function for image frame t_j and H is the Heaviside function. Because voxel intensities are assumed to be constant over the time, the unknown density functions p_{obj} and p_{bg} are estimated using the reference segmentation and intensity values of the reference frame. Under the assumption that initial segmentations lie near the object boundary only voxels in a certain region around the object are used for a parzen–window estimation[37] of intensity probabilities:

$$p_j(g) = \frac{1}{|G_j|} \sum_{g_i \in G_j} \frac{1}{\sigma\sqrt{2\pi}} \exp\left(-\frac{(g - g_i)^2}{2\sigma^2}\right) \text{ with } j \in \{\text{"obj"}, \text{"bg"}\}$$

$$\text{and} \quad G_{obj} = \{I(\boldsymbol{x}, t_{ref}) | d_{low} < -\Phi_{ref}(\boldsymbol{x}) < d_{high}\}$$

$$G_{bg} = \{I(\boldsymbol{x}, t_{ref}) | d_{low} < \Phi_{ref}(\boldsymbol{x}) < d_{high}\}.$$

The lower distance threshold d_{low} is used to be more robust against segmentation errors and partial volume effects. Fig. 1 shows estimated density functions for background and liver and an example CT image slice

overlayed with the segmentation result using eq. (1). It can be observed that due to overlapping intensity ranges an intensity based liver segmentation will fail. Therefore, additional shape prior information is needed.

Different approaches were developed for incorporating prior shape knowledge into level set based segmentation methods.[10, 38, 39] In our approach, the similarity between shapes is evaluated by the distance of the zero level set of Φ_j to the reference shape Φ_{ref}:

$$\int_\Omega \delta(\Phi_j(\boldsymbol{x})) \left(\Phi_j(\boldsymbol{x}) - (\Phi_{ref} \circ \boldsymbol{\varphi})(\boldsymbol{x})\right)^2 \ d\boldsymbol{x}. \tag{2}$$

$\delta(\cdot)$ denotes the Dirac distribution and $\Phi_{ref} \circ \boldsymbol{\varphi}$ applies a transformation $\boldsymbol{\varphi}$ to the reference shape. The formulation in eq. (2) has the advantage that the level set function Φ_j has to be evaluated only near the zero level set, that corresponds to efficient implementation techniques, like sparse fields or narrow bands. Furthermore, we seek for a transformation $\boldsymbol{\varphi}$ that best match the reference shape to the current target image. This transformation is determined by a registration of the reference frame $I(\boldsymbol{x}, t_{ref})$ with the current target frame $I(\boldsymbol{x}, t_j)$.

2.2 Variational framework for joint segmentation and motion estimation.

Due to the wide range of applications a variety of different registration techniques has been developed in the last two decades (see Zitova and Flusser (2003)[40] for an survey). In our application a dense non-linear displacement field is needed. Therefore, we will focus on non–linear intensity–driven approaches. The aim of image registration is to find a transformation $\boldsymbol{\varphi}(\boldsymbol{x}) = \boldsymbol{x} - \boldsymbol{u}(\boldsymbol{x})$ that matches the reference frame $I_{ref} \circ \boldsymbol{\varphi}$ onto the target frame I_j. The general registration problem may be phrased as:[34] $\mathcal{J}^{Reg}[\boldsymbol{u}] = \mathcal{D}[I_{ref}, I_j; \boldsymbol{u}] + \alpha \mathcal{S}[\boldsymbol{u}] \rightarrow \min$, where $\mathcal{D}$ models the distance measure, e.g. sum of squared differences (SSD) or mutual information, and $\mathcal{S}$ is a regularizer to constrain the calculated transformation to physically meaningful movements. We choose the sum of squared differences to measure intensity differences and the diffusive regularization to ensure a smooth deformation field. Diffusive regularization was used in different applications for optical flow estimation[20, 41] and leads to a very efficient numerical implementation.[42]

The aim is to find the level set segmentation Φ_j of the target frame $I(\boldsymbol{x}, t_j)$ and the displacement field $\boldsymbol{u}_j(\boldsymbol{x})$ between I_j and I_{ref} simultaneously by minimizing the energy functional:

$$
\begin{aligned}
\mathcal{J}[\Phi_j, \boldsymbol{u}_j] \ = \ & \lambda_1 \underbrace{\int_\Omega -H(\Phi_j(\boldsymbol{x})) \log\left(p_{bg}(I(\boldsymbol{x}, t_j))\right) - (1 - H(\Phi_j(\boldsymbol{x}))) \log\left(p_{obj}(I(\boldsymbol{x}, t_j))\right) \ d\boldsymbol{x}}_{\text{intensity–based segmentation}} \\[2mm]
& + \lambda_2 \underbrace{\int_\Omega \|\nabla H(\Phi_j(\boldsymbol{x}))\| \ d\boldsymbol{x}}_{\text{contour length}} \\[2mm]
& + \lambda_3 \underbrace{\int_\Omega \left(I(\boldsymbol{x}, t_j)) - I(\boldsymbol{x} - \boldsymbol{u}_j(\boldsymbol{x}), t_{ref})\right)^2 \ d\boldsymbol{x}}_{\text{intensity–based registration}} \\[2mm]
& + \lambda_4 \underbrace{\frac{1}{2} \sum_{l=1}^{d} \int_\Omega \|\nabla \boldsymbol{u}_{jl}\|^2 \ d\boldsymbol{x}}_{\text{diffusive regularization}} \\[2mm]
& + \lambda_5 \underbrace{\int_\Omega \delta(\Phi_j(\boldsymbol{x})) \left(\Phi_j(\boldsymbol{x}) - \Phi_{ref}(\boldsymbol{x} - \boldsymbol{u}_j(\boldsymbol{x}))\right)^2 \ d\boldsymbol{x}}_{\text{shape prior}}
\end{aligned}
\tag{3}
$$

Here, the segmentation and registration processes are coupled by the shape prior term. The energy functional $\mathcal{J}$ is minimized with respect to $\boldsymbol{u}_j$ and Φ_j for each desired time frame $I(\boldsymbol{x}, t_j)$. λ_i, $(i = 1, \ldots, 5)$ are parameters balancing the influence of the five terms in the model.

In contrast to other approaches for joint segmentation and non-linear registration[19, 20] the displacement field $\boldsymbol{u}$ is determined for the whole image domain and not only between object surfaces. In regions distant from the contour the displacements are influenced mainly by image intensities. Near the object surface the influence of the coupling term grows. However, due to the smoothing criterion the segmentation information may affect the transformation in a large image region.

The shape prior term penalizes distances between Φ_j and the deformed reference shape. In contrast to other approaches,[14, 20] deviations between Φ_j and $\Phi_{ref} \circ \boldsymbol{\varphi}$ are possible depending on the weighting parameter λ_5. The reason for this approach is two-fold: First, the segmentation result becomes resistant to small segmentation errors in the reference shape. Furthermore, current non–linear registration methods presume smooth continuous deformation fields, but complex deformations of inner organs are sometimes non–continuous (e.g. motion of the lung along the pleura). Therefore, a correct registration is not possible in every case. By choosing a variable weighting parameter $\lambda_5(\boldsymbol{x})$ in eq. (3) prior knowledge about problematic regions can be incorporated in the model. A drawback of this approach is that the level set function Φ_j is not fully determined by the displacement field $\boldsymbol{u}_j$ and additional unknowns must be calculated. However, the level set segmentation can be computed very efficiently and the additional computation time is negligible (see section 2.3).

2.3 Numerical Methods.

In the numerical implementation continuous approximations δ_ϵ and H_ϵ of the Dirac and Heaviside distributions are used.[12] For the minimization of eq. (3) a time marching approach was employed. According to the calculus of variations a solver of eq. (3) must fulfill the conditions:

$$\frac{\partial \mathcal{J}}{\partial \Phi_j} = 0 \quad \text{and} \quad \frac{\partial \mathcal{J}}{\partial \boldsymbol{u}_j} = 0. \tag{4}$$

From the associated Euler–Lagrange equations the following iterative update scheme is derived:

$$
\begin{aligned}
\Phi_j^{k+1} = \Phi_j^k \quad &+ \quad \tau_\phi \, \lambda_1 \delta_\epsilon(\Phi_j^k) \left(\log(p_{bg}(I_j(\boldsymbol{x}))) - \log(p_{obj}(I_j(\boldsymbol{x}))) \right) \\
&- \quad \tau_\phi \, \lambda_2 \delta_\epsilon(\Phi_j^k) \nabla \cdot \frac{\nabla \Phi_j^k}{|\nabla \Phi_j^k|} \\
&+ \quad \tau_\phi \, \lambda_5 \delta_\epsilon(\Phi_j^k) \, \left(\Phi_j^k(\boldsymbol{x}) - \Phi_{ref}(\boldsymbol{x} - \boldsymbol{u}_j) \right)
\end{aligned}
\tag{5}
$$

and

$$
\begin{aligned}
\boldsymbol{u}_j^{k+1} - \tau_u \Delta \boldsymbol{u}_j^{k+1} = \boldsymbol{u}_j^k \quad &+ \quad \tau_u \, \lambda_2 \left(I_j(\boldsymbol{x}) - I_{ref}(\boldsymbol{x} - \boldsymbol{u}_j^k) \right) \nabla I_{ref}(\boldsymbol{x} - \boldsymbol{u}_j^k) \\
&+ \quad \tau_u \, \lambda_5 \delta_\epsilon(\Phi_j) \left(\Phi_j(\boldsymbol{x}) - \Phi_{ref}(\boldsymbol{x} - \boldsymbol{u}_j^k) \right) \nabla \Phi_{ref}(\boldsymbol{x} - \boldsymbol{u}_j^k),
\end{aligned}
\tag{6}
$$

where k is the current iteration number and τ_ϕ, τ_u denote the size of the time steps. In each iteration step Φ_j is updated according to eq. (5) and $\boldsymbol{u}_j$ is updated according to eq. (6) until a steady state solution of both evolution equations is found. Sparse field level sets[43] are used for an efficient computation of Φ_j. In eq. (6) an efficient semi–implicit iteration scheme is utilized using additive operator splitting for the necessary matrix inversion.[42] Assuming $t_{ref} = t_0$, the calculated displacement for time frame j is used to initialize the next time frame: $\boldsymbol{u}_{j+1}^0 = \boldsymbol{u}_j$ and $\Phi_{j+1}^0(\boldsymbol{x}) = \Phi_{ref}(\boldsymbol{x} - \boldsymbol{u}_j)$ and $\boldsymbol{u}_0 = \boldsymbol{0}$.

3. EXPERIMENTS AND RESULTS

3.1 Image acquisition and validation methods

The behavior of the algorithm was investigated by segmenting the liver in 4D CT image sequences acquired during free breathing. Four cancer patients were examined with a 16-slice CT scanner (Brilliance, Philips Medical Systems, Cleveland) operated in cine-mode for the investigation of respiration-induced organ mobility. During the acquisition process the patients were instructed to breathe naturally. For each patient 25 scans per couch position were acquired continuously, 16 to 19 couch positions were investigated to ensure adequate coverage of the thorax and upper abdomen. For further data acquisition details see Low et al.(2003)[44] and Lu et al.(2005).[45]

<div style="text-align:center">(a)   (b)   (c)</div>
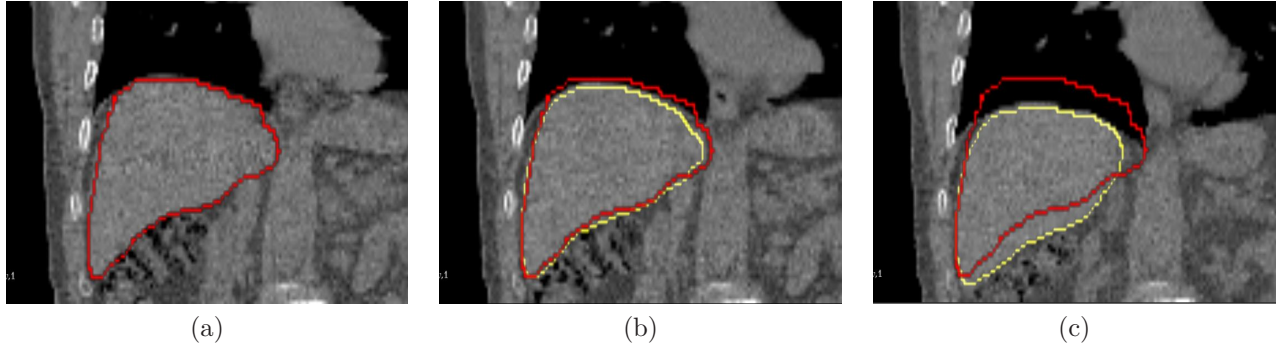
Figure 2. Automatic liver segmentation in 4D CT data using joint segmentation and registration. Left: reference phase of the respiratory cycle with reference segmentation shown in red. Middle and Right: results for two frames of the image sequence with the automatic re-contouring results shown as yellow curves (the reference liver contour is shown in red).

The resulting spatiotemporal series of CT scans were used to reconstruct 4D CT data sets. To reduce artifacts which were caused by sorting based 4D reconstruction methods[45] an optical flow based reconstruction method for 4D data sets was applied.[24, 46] The resulting artifact–reduced reconstructed 4D CT data sets consist of 14 3D images consisting of $512 \times 512 \times 272$ voxel. In contrast to diagnostic CT protocols the exposure per slice has to be significantly reduced due to the large number of slices (about 3800 slices per patient). Therefore, the resulting 4D images are characterized by a poor soft tissue contrast and segmentation of inner organs, like liver or pancreas, becomes challenging (see fig 1).

For each patient data set 6 time frames were selected: maximum inhalation, maximum exhalation, two intermediate frames during inhalation and two frames in the exhalation phase. The liver was segmented by an expert in each of the associated 24 image volumes as ground truth. The joint segmentation and registration algorithm was applied for the automatic re-contouring of the 4D CT data. The peak exhale image is treated as reference and used to segment the liver contour in the remaining 5 image volumes for each patient.

For comparison purpose, three different experiments were performed : in a first experiment, we register reference and target image by a diffusive registration approach ($\lambda_1 = \lambda_2 = \lambda_5 = 0$). The segmentation result is the deformed reference segmentation (algorithm "pure Reg"). In a second experiment, the result of the registration step is improved by a succeeding level set segmentation with $\lambda_3 = \lambda_4 = 0$ using the deformed reference segmentation as shape prior information (algorithm "Reg→Seg"). In the last experiment, we perform the proposed joint segmentation and registration by minimizing eq. (3) (algorithm: "joint Reg+Seg").

To evaluate segmentation accuracy, mean surface distances and overlap coefficients were computed between the ground truth and the segmentation results of the three algorithms (pure Reg, Reg→Seg and joint Reg+Seg). The overlap coefficient is defined as $\frac{|A \cap B|}{|A \cup B|}$, where A and B are the automatically estimated region and the corresponding manually segmented ground truth. There is no ground truth available for the validation of estimated displacement fields. We computed the mean squared intensity difference (MSD) between the warped reference image and the target image frame and validated registration accuracy by visual inspection.

3.2 Results

The necessary parameters were determined experimentally for one image pair and we reused this set of parameters for all tests. The parameters used in our tests are: $\tau_u = \tau_\phi = 0.5$, $\lambda_1 = 0.2$, $\lambda_2 = 0.3$, $\lambda_3 = 1$, $\lambda_4 = 0.5$ and $\lambda_5 = 0.1$ (except $\lambda_i = 0$ as described above).

In figure 2 three images acquired in different phases of the respiratory cycle are shown. Figure 2(a) presents the reference image for patient A and the manual liver segmentation is illustrated as red curve. The liver region in all other phases is automatically segmented using the proposed joint registration and segmentation method. The results for two frames of the image sequence are shown in figure 2(b) and 2(c). By visual inspection, the results are very accurate despite large deformations. Table 1 and 2 summarize the results of the segmentation accuracy. The presented mean surface distances and overlap coefficients are averaged over all time frames per

	pure Reg	*Reg→Seg*	*joint Reg+Seg*
Patient A	92,45%	94,01%	94.71%
Patient B	93,04%	89,00%	94,46%
Patient C	92,09%	91,91%	93,96%
Patient D	92,88%	91,41%	94,98%

Table 1. Overlap coefficients (in %) between the ground truth and the segmentation maps obtained using diffusive registration (*pure Reg*), registration and subsequent segmentation (*Reg→Seg*) and combined registration and segmentation (*joint Reg+Seg*). All values are averaged over five breathing phases.

	pure Reg	*Reg→Seg*	*joint Reg+Seg*
Patient A	1,31	1,78	1,15
Patient B	1,19	2,25	1,14
Patient C	1,63	1,66	1,38
Patient D	1,45	1,58	1,26

Table 2. Mean surface distances (in mm) between the ground truth and the segmentation result obtained using diffusive registration (*pure Reg*), registration and subsequent segmentation (*Reg→Seg*) and combined registration and segmentation (*joint Reg+Seg*). All values are averaged over five breathing phases.

patient. It can be observed that combined registration and segmentation leads to the best segmentation results for all test cases. For three patients, the subsequent segmentation in the *Reg→Seg* algorithm leads to a decrease in the segmentation performance due to contour leakage.

Fig. 3 visualize segmentation accuracy of the three methods for each time frame of patient D. If reference and target frame are close together, joint registration/segmentation and pure registration have a similar segmentation performance. If the differences between reference and target get more apparent, joint registration/segmentation perform considerably better. Furthermore, the graph reveals the advantages and disadvantages of subsequent registration and segmentation. One the one hand, contour leakage cause decreased segmentation performance if registration–based segmentation results are very accurate. On the other hand, segmentation performance is enhanced due to the succeeding adaptation of the contour if no accurate registration can be achieved.

In fig. 4 an example of the iterative decrease of mean squared differences between target image and deformed reference image by standard registration and by joint registration/segmentation is shown. Due to low intensity differences between liver and surrounding tissues, the registration converges very slow in this region. It can be observed that the additional segmentation information leads to a faster convergence of the registration method. However, by visual inspection the final registration results are very similar between standard registration and joint registration/segmentation.

4. CONCLUSION

This paper presents a variational approach for simultaneous segmentation and registration applied to temporal image sequences. The proposed method starts with a known segmentation in one frame and then recovers
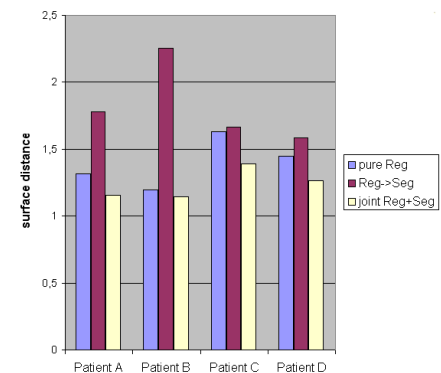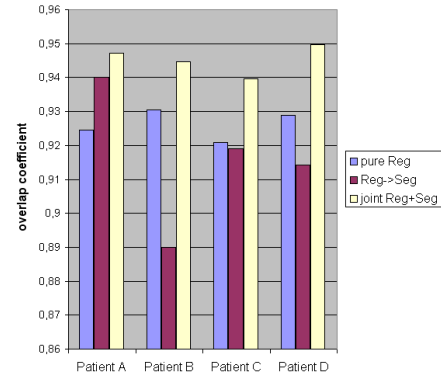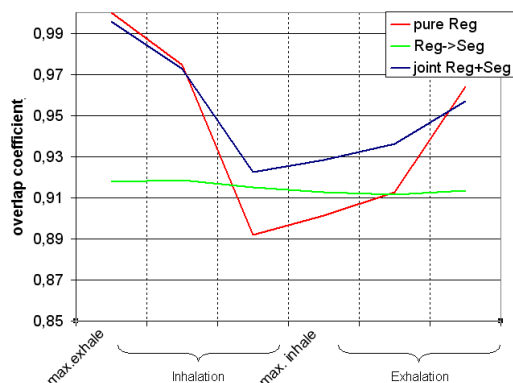
Figure 3. Evaluation results of segmentation accuracy for each time frame of patient D.
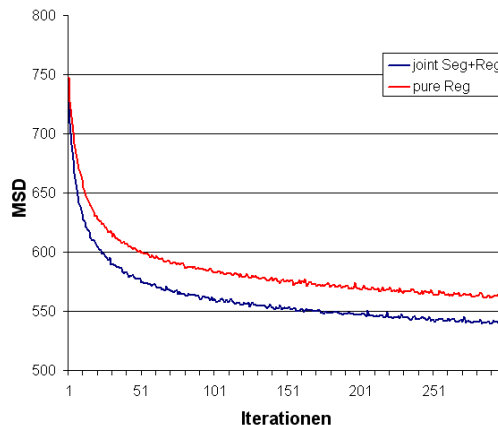
Figure 4. Example curve for the decrease of the mean squared difference between target image and deformed reference image during joint registration/segmentation.

non-linear registration and segmentation in other frames by minimizing a cost function that combines intensity-based registration, level-set segmentation and prior shape knowledge. The purpose of the presented method is to estimate respiration induced organ motion in spatiotemporal CT image sequences and to segment a structure of interest simultaneously. Experimental results using temporal CT image sequences showed that the proposed approach performed better than two other segmentation/registration schemes: standard registration of reference and target image or registration and subsequent segmentation. Furthermore, the proposed method can be implemented efficiently using sparse field level sets and additive operator splitting. We consider that the presented method holds the potential to asses the respiratory dynamic of inner organs and can be used to outline automatically structures of interest in 4D image data for radiotherapy planning.

The current implementation contains no temporal smoothness condition for displacement field or segmentation. This is due to the size of the considered data sets and due to run–time and memory issues. However, the inclusion of such conditions in our approach is straight forward. A drawback of our method is that 7 parameters have to be defined: $\lambda_1, \ldots, \lambda_5, \tau_\phi$ and τ_u. However, compared to registration and succeeding segmentation only one additional parameter is needed for combined segmentation and registration. In future work we will investigate the automatic determination of the parameters.

Validation of nonrigid registration algorithms is difficult and is an current area of research. Visual assessment of the registration results indicated that both registration algorithms are able to determine adequate respiratory motion and organ deformation. Future work includes more thorough validation of registration accuracy. Therefore, the presented method will be evaluated using software phantoms[47] with known displacement fields or patient data sets with extracted landmark trajectories.

REFERENCES

1. P. J. Keall, G. Mageras, J. M. Balter, *et al.*, "The management of respiratory motion in radiation oncology report of aapm task group 76," *Medical physics* **33**(10), pp. 3874–3900, 2006.
2. A. Schweikard, G. Glosser, M. Bodduluri, M. J. Murphy, and J. R. Adler, "Robotic motion compensation for respiratory movement during radiosurgery," *Comput Aided Surg* **5**, pp. 263–77, 2000.
3. S. S. Vedam, P. J. Keall, A. Docef, D. A. Todor, V. R. Kini, and R. Mohan, "Predicting respiratory motion for four-dimensional radiotherapy," *Med. Phys.* **31**, pp. 2274–2283, Aug 2004.
4. T. Rohlfing, C. R. Maurer, W. G. O'Dell, and J. Zhong, "Modeling liver motion and deformation during the respiratory cycle using intensity-based nonrigid registration of gated MR images.," *Med Phys* **31**, pp. 427–432, Mar 2004.

5. R. Werner, J. Ehrhardt, T. Frenzel, D. Säring, W. Lu, D. Low, and H. Handels, "Motion artifact reducing reconstruction of 4D CT image data for the analysis of respiratory dynamics," *Methods of Information in Medicin* **49**, pp. 254–260, 2007. (IF: **0.970** (2005)).

6. L. Weruaga, J. Morales, L. Nez, and R. Verd, "Estimating volumetric motion in human thorax with parametric matching constraints.," *IEEE Trans Med Imaging* **22**, pp. 766–772, Jun 2003.

7. D. Sarrut, V. Boldea, M. Ayadi, J.-N. Badel, C. Ginestet, S. Clippe, and C. Carrie, "Nonrigid registration method to assess reproducibility of breath-holding with ABC in lung cancer.," *Int J Radiat Oncol Biol Phys* **61**, pp. 594–607, Feb 2005.

8. R. Werner, J. Ehrhardt, R. Schmidt, and H. Handels, "Modeling respiratory lung motion - a biophysical approach using finite element methods," in *SPIE Medical Imaging 2008*, (San Diego), 2008. (accepted).

9. J. Ehrhardt, R. Werner, T. Frenzel, W. Lu, D. Low, and H. Handels, "Analysis of free breathing motion using artifact reduced 4D CT image data," in *SPIE Medical Imaging 2007*, J. M. Reinhardt and P. W. Pluim, eds., **6512**, pp. 1N1–8, (San Diego), 2007.

10. Y. Chen, H. Tagare, S. Thiruvenkadam, F. Huang, D. Wilson, K. Gopinath, R. Briggs, and E. Geiser, "Using prior shapes in geometric active contours in a variational framework," *Int. J. Comp. Vis.* **50**(3), pp. 315–328, 2002.

11. B. Flach, E. Kask, D. Schlesinger, and A. Skulish, "Unifying registration and segmentation for multi-sensor images," in *Pattern Recognition*, *LNCS* **2449**, pp. 190–197, Springer, 2002.

12. N. Paragios, "A level set approach for shape-driven segmentation and tracking of the left ventricle," *IEEE Trans. Med. Imag.* **22**, pp. 773–776, June 2003.

13. P. Wyatt and J. A. Noble, "Map mrf joint segmentation and registration of medical images," *Med Image Anal* **7**(4), pp. 539–552, 2003.

14. A. Yezzi, L. Zollei, and T. Kapur, "A variational framework for integrating segmentation and registration through active contours," *Med Imag Anal* **7**(2), pp. 171–185, 2003.

15. Y. Young and D. Levy, "Registration-base morphing of active contours for segmentation of ct scans," *Math. Biosci. Eng.* **2**, pp. 79–96, 2005.

16. J. Ashburner and K. Friston, "Unified segmentation," *NeuroImage* **26**, pp. 839–851, 2005.

17. E. D'Agostino, F. Maes, D. Vandermeulen, and P. Suetens, "A unified framework for atlas based brain image segmentation and registration.," in *Biomedical Image Registration, WBIR 2006*, J. P. W. Pluim, B. Likar, and F. A. Gerritsen, eds., *LNCS* **4057**, pp. 136–143, Springer, 2006.

18. D. Cremers and S. Soatto, "Motion competition: A variational approach to piecewise parametric motion segmentation," *Int J Comp Vision* **62**(3), pp. 249–265, 2005.

19. J.-h. An, Y. Chen, F. Huang, D. C. Wilson, and E. A. Geiser, "A variational PDE based level set method for a simultaneous segmentation and non-rigid registration.," in *MICCAI*, J. S. Duncan and G. Gerig, eds., *LNCS* **3749**, pp. 286–293, Springer, 2005.

20. G. Unal and G. Slabaugh, "Coupled PDEs for non-rigid registration and segmentation," in *Computer Vision and Pattern Recognition, Computer Vision and Pattern Recognition, 2005. CVPR 2005. IEEE Computer Society Conference on* **1**, pp. 168–175, June 2005.

21. T. Brox, T. Brox, and J. Weickert, "Level set segmentation with multiple regions," **15**(10), pp. 3213–3218, 2006.

22. D. Cremers and S. Soatto, "Variational space-time motion segmentation," in *Computer Vision, 2003. Proceedings. Ninth IEEE International Conference on*, pp. 886–893vol.2, 13-16 Oct. 2003.

23. D. Mumford and J. Shah, "Optimal approximation by piecewise smooth functions and associated variational problems," *Comm. Pure Applied Math* **42**, pp. 577–685, 1989.

24. J. Ehrhardt, R. Werner, D. Säring, T. Frenzel, W. Lu, D. Low, and H. Handels, "An optical flow based method for improved reconstruction of 4D CT data sets acquired during free breathing," *Medical Physics* **34**(2), pp. 711–721, 2007.

25. H. Handels, R. Werner, R. Schmidt, T. Frenzel, W. Lu, D. Low, and J. Ehrhardt, "4d medical image computing and visualization of lung tumor mobility in spatio-temporal ct image data," *Int J Medical Informatics* **76**, 2007. (in press).

26. A. Schenk, G. Prause, and H. O. Peitgen, "Efficient demiautomatic segmentation of 3d objects," in *Medical Image Computing and Computer-Assisted Intervention - MICCAI 2000, LNCS* **1935**, pp. 186–195, Springer, 2000.

27. S. Pan and B. M. Dawant, "Automatic 3D segmentation of the liver from abdominal CT images: a level-set approach," in *Proc. SPIE Medical Imaging 2001: Image Processing*, M. Sonka and K. M. Hanson, eds., **4322**, pp. 128–138, July 2001.

28. F. Liu, B. Zhao, P. K. Kijewski, L. Wang, and L. H. Schwartz, "Liver segmentation for ct images using gvf snake," *Medical Physics* **32**(12), pp. 3699–3706, 2005.

29. S.-J. Lim, Y.-Y. Jeong, and Y.-S. Ho, "Automatic liver segmentation for volume measurement in ct images," *J Vis Comm Image Repr* **17**(4), pp. 860–875, 2006.

30. J. Lee, N. Kim, H. Lee, J. B. Seo, H. J. Won, Y. M. Shin, and Y. G. Shin, "An automatic method for fast and accurate liver segmentation in ct images using a shape detection level set method," in *Medical Imaging 2007: Image Processing*, J. P. W. Pluim and J. M. Reinhardt, eds., **6512**(1), p. 65122V, SPIE, 2007.

31. R. Malladi, J. Sethian, and B. Vemuri, "Shape modeling with front propagation: A level set approach," *IEEE Transactions on Pattern Analysis and Machine Intelligence* **17**(2), pp. 158–174, 1995.

32. J. A. Sethian, *Level Set Methods: Evolving Interfaces in Geometry, Fluid Mechanics, Computer Vision, and Materials Science*, Cambridge University Press, 1996.

33. T. Chan and L. Vese, "Active contours without edges," *IEEE Trans. Med. Imag.* **10**, pp. 266–277, Feb. 2001.

34. J. Modersitzki, *Numerical Methods for Image Registration*, Oxford University Press, 2003.

35. N. Paragios and R. Deriche, "Unifying boundary and region-based information for geodesic active tracking," in *Computer Vision and Pattern Recognition*, **2**, 23-25 June 1999.

36. M. Rousson and R. Deriche, "A variational framework for active and adaptative segmentation of vector valued images," in *Proc. Workshop on Motion and Video Computing*, pp. 56–61, 5–6 Dec. 2002.

37. R. Duda and P. Hart, *Pattern Classification and Scene Analysis*, John Wiley & Sons, Inc., 1973.

38. M. Rousson and N. Paragios, "Shape priors for level set representations," in *ECCV '02: Proceedings of the 7th European Conference on Computer Vision-Part II*, pp. 78–92, Springer-Verlag, (London, UK), 2002.

39. D. Cremers and S. Soatto, "A pseudo-distance for shape priors in level set segmentation," in *2nd IEEE Workshop on Variational , Geometric and Level Set Methods in Computer Vision*, N. Paragios, ed., (Nice), 2003.

40. B. Zitova and J. Flusser, "Image registration methods: A survey," *Image and Vision Computing* **21**(11), pp. 977–1000, 2003.

41. A. Bruhn and J. Weickert, "Towards ultimate motion estimation: combining highest accuracy with real-time performance," in *Proc. Tenth IEEE International Conference on Computer Vision ICCV 2005*, **1**, pp. 749–755, 17–21 Oct. 2005.

42. B. Fischer and J. Modersitzki, "A super fast registration algorithm," in *Bildverarbeitung für die Medizin*, pp. 169–173, 2001.

43. R. T. Whitaker, "A level-set approach to 3d reconstruction from range data," *Int. J. Comput. Vision* **29**(3), pp. 203–231, 1998.

44. D.-A. Low, M. Nystrom, E. Kalinin, P. Parikh, J.-F. Dempsey, J.-D. Bradley, S. Mutic, S.-H. Wahab, T. Islam, G. Christensen, D.-G. Politte, and B.-R. Whiting, "A method for the reconstruction of four-dimensional synchronized CT scans acquired during free breathing," *Med. Phys.* **30**(6), pp. 1254–1263, 2003.

45. W. Lu, P. J. Parikh, I. M. El Naqa, M. M. Nystrom, J. P. Hubenschmidt, S. H. Wahab, S. Mutic, A. K. Singh, G. E. Christensen, J. D. Bradley, and D. A. Low, "Quantitation of the reconstruction quality of a four-dimensional computed tomography process for lung cancer patients," *Med. Phys.* **32**, pp. 890–901, 2005.

46. J. Ehrhardt, R. Werner, T. Frenzel, D. Säring, W. Lu, D. Low, and H. Handels, "Reconstruction of 4D-CT data sets acquired during free breathing for the analysis of respiratory motion," in *SPIE Medical Imaging 2006*, J. M. Reinhardt and P. W. Pluim, eds., **6144**, pp. 2141–8, (San Diego), 2006.

47. W. Segars, D. Lalush, and B. Tsui, "Modeling respiratory mechanics in the mcat and spline-based mcat phantoms," *IEEE Trans Nuclear Science* **48**, pp. 89–97, Feb 2001.